Theoretical approach to δ doping of GaAs with In

Steffen Wilke and Dieter Hennig
Department of Physics, Humboldt-University Berlin, Invalidenstrasse 110, O-1040 Berlin, Germany
(Received 21 December 1990)

A systematic study of the electronic structure at In-δ-doping layers embedded into GaAs or into the well region of AlAs/GaAs quantum wells is presented. The electronic structure is calculated within the framework of a tight-binding scheme using surface Green-function techniques. We describe the Koster-Slater approach to δ doping and discuss the behavior of deep levels induced near the conduction-band edge for single and double δ doping of GaAs with In. It is shown that the trends in level position are connected with the quasi-one-dimensional nature of the Green function near the conduction-band edge. In the case in which the δ-doping layer is arranged inside the GaAs well region of an AlAs/GaAs quantum well, it is shown that the level positions are sensitive to the distance between the δ-doping layer and the interfaces but show no dependence on the changed local electronic structure in GaAs.

I. INTRODUCTION

An interesting development in modern growth technology is the possibility to embed single layers of impurity atoms (called δ-doping layers) inside a host material. Such systems have been reported for δ doping with shallow impurities as well as for δ doping by isoelectronic substitution.[1–6] In this paper we are concerned with isoelectronic δ doping.

Photoluminescence spectra of δ doping of GaAs with In have shown intense sharp lines redshifted with respect to the GaAs bulk spectrum.[1–5] The position of peaks has been altered by changing the coverage and thickness of the δ-doping planes as well as by introducing a second δ-doping layer some distance from the first.

Isoelectronic δ doping and the analysis of the corresponding photoluminescence spectra are interesting in several respects. In isoelectronic substitution both types of atoms have similar chemical properties but differ in general by their covalent radii and atomic level positions. Therefore no extra free carriers and strong long-ranged Coulomb fields are introduced and the impurity potential is localized. The different covalent radii and hence the differing lattice constants of the host structure and the corresponding crystal formed by the impurity atoms lead to large internal strain fields. The difference of bulk lattice constants between GaAs and InAs amounts to 7.16%. In the heteroepitaxy of those structures the similar chemical properties make a variation of the coverage of the δ-doping plane with impurities in the whole range from 0 to 1 possible but the large internal strain fields allow for critical thicknesses of isomorphic growth of only a few monolayers.[2]

The electronic structure of δ-doped GaAs and the formation of impurity levels well separated from the GaAs band edges have mostly been interpreted viewing δ doping as the limiting case of ultrathin quantum wells. Even a simple effective-mass, square-well model described the experimental results for single monolayer δ doping fairly well.[4,5] Recent pseudopotential calculations[7] of the energy gap in double δ-doped GaAs corrected those results only slightly and achieved a good fit to experimental results. But, on the other hand, δ doping mediates between single impurities and quantum wells.[8] Within the impurity picture δ doping is the limit of large planar impurity clusters. A single In impurity in GaAs does not induce a deep level. It is therefore interesting to study the electronic structure of various δ-doping arrangements in more detail.

The object of this paper is the electronic structure near the conduction-band edge for different arrangements of In δ-doping planes in GaAs. Beside δ doping of pure GaAs we discuss the case where the δ-doping plane is embedded in the well region of an AlAs-GaAs-AlAs quantum well in different distances to the heterointerfaces. The theoretical method is based on a tight-binding approximation. It is known to give correct semiquantitative trends in the electronic structure of impurities as well as for superlattices, heterostructures, and quantum wells.

The paper is organized as follows. In Sec. II we describe the theoretical model and the Koster-Slater approach to δ doping. The last part of Sec. II explains the calculation procedure in more detail. The results are collected in Sec. III.

II. THEORY

A. The model

In our study of δ doping of GaAs with In we consider different arrangements of δ-doping layers inside a host material. This may be pure GaAs, as used in recent experiments, but we consider also AlAs-GaAs-AlAs single quantum wells. The double δ-doping arrangement of two impurity monolayers separated by n monolayers of GaAs is considered in pure GaAs only. All structures are assumed to be grown along the [001] direction.

The local atomic arrangement in δ-doped structures

deviates generally from that of a simple substitution of host atoms by impurities. Most important is the biaxial deformation of the δ-doping layers due to different lattice constants of the δ-doping material and the host. The biaxial strain field can be divided into a hydrostatic contribution changing the atomic volume and a tetragonal distortion connected in general with a symmetry reduction in comparison to the relaxed pure crystal. Because the conduction-band edge in InAs is formed by a nondegenerate highly dispersive band around the Γ point it is affected mainly by the hydrostatic component. In contrast, at the valence-band edge both components have to be considered. In this paper we confine ourselves to an energy region near the conduction-band edge and may therefore neglect the tetragonal distortion. The hydrostatic shift of the conduction-band edge is included in the parametrization of the InAs band structure. Other deviations as caused by nonideal pseudosmooth interfaces or noninteger coverages may be important for explaining details of the photoluminescence spectrum.[5] Neglecting the actual atomic arrangement and fluctuations of step sizes, impurity concentration, cluster sizes, etc., we approximate a noninteger coverage and a small interdiffusion of impurity atoms by averaged impurity concentrations inside every δ-doping layer. In consequence, within this model the averaged atomic arrangement perpendicular to the growth direction remains periodic.

The electronic structure is calculated using a tight-binding model with interaction range restricted to second-nearest neighbors. The basis of the parametrization of the Hamilton matrix for the three structures GaAs, InAs, and AlAs has been taken from Ref. 9. To parametrize heterostructures and impure systems it is important to define a relationship between the pure crystal parameters and those inside the composed structure. The concept of band offsets to relate the bands of heterojunction components on an absolute energy scale can be applied to the GaAs-AlAs interface and thicker δ-doping layers but it is not to be used straightforwardly for layers only a few monolayers thick. Here, a transition to the impurity picture, where atomic level differences are the basis in defining matrix elements of the impurity potential, is expected. With regard to the semiquantitative character of our description and the uncertainties in the value of the band offsets and the impurity potential matrix elements, we use, in accordance with the literature,[10] the conduction-band offset of strained InAs to place the InAs band structure in relation to GaAs. The actual value has been set to $\Delta E_c = 0.79$ eV. The resulting parameters and the eigenvalues of the lowest conduction band at the points Γ, X, and L are given in Table I. As usual, the energy zero is set to the valence-band top of GaAs.

TABLE I. Parametrization of GaAs, AlAs, and InAs band structure and the eigenvalues of the lowest conduction band at points Γ, X, and L. All values in eV.

	GaAs	AlAs	InAs
$E_{ss}(000)_0$	−8.182	−8.182	−8.182
$E_{ss}(000)_1$	−3.808	−2.808	−2.800
$E_{xx}(000)_0$	0.191	0.191	0.191
$E_{xx}(000)_1$	3.165	2.600	3.800
$4E_{ss}(\frac{1}{2}\frac{1}{2}\frac{1}{2})$	−6.577	−6.900	−6.175
$4E_{sx}(\frac{1}{2}\frac{1}{2}\frac{1}{2})_{01}$	4.040	4.700	4.000
$4E_{sx}(\frac{1}{2}\frac{1}{2}\frac{1}{2})_{10}$	4.259	3.200	4.100
$4E_{xx}(\frac{1}{2}\frac{1}{2}\frac{1}{2})$	1.309	2.000	1.100
$4E_{xy}(\frac{1}{2}\frac{1}{2}\frac{1}{2})$	4.877	4.877	4.459
$4E_{xx}(011)_0$	−0.202	−0.202	−0.202
$4E_{xx}(011)_1$	−0.877	−0.877	−1.035
$4E_{xy}(110)_0$	0.317	0.317	0.317
$4E_{xy}(110)_1$	0.376	0.376	0.67
$4E_{xx}(110)_0$	0.212	0.212	0.212
$4E_{xx}(110)_1$	0.924	0.924	0.952
$4E_{sx}(100)_0$	0.0	0.0	0.0
$4E_{sx}(110)_1$	0.0	0.0	0.0
$4E_{ss}(110)_0$	0.059	0.059	0.059
$4E_{ss}(110)_1$	0.257	0.257	−0.284
$4E_{sx}(011)_0$	1.203	1.203	1.203
$4E_{sx}(011)_1$	−0.058	0.0	0.497
Γ	1.51	2.50	0.72
X	2.03	1.71	2.37
L	1.81	1.96	1.53

B. Density of states

To calculate the spectrum of nonperiodic structures, we use the Green-function formalism. The central quantities to describe the spectral properties are projected densities of states that contain information about the energy as well as about the spatial distribution of states.[11–13] The projected density of states (PDOS) is directly related to diagonal matrix elements of the Green-function matrix.

Within the tight-binding formalism we start with elements of the Hamilton matrix related to a localized basis $|I\alpha\rangle$ of orbitals α centered at an atom at position $\mathbf{R}_I$. This basis is used to describe the electronic spectrum in nonperiodic structures as, e.g., that near a single impurity. In structures showing a two-dimensional periodicity a mixed representation $|\mathbf{K}i\alpha\rangle$ is more suited. Owing to this periodicity two-dimensional Bloch waves with the wave vector $\mathbf{K}$ are introduced. Along the growth direction the local description labeled by the layer index i is retained.

Defining the one-particle Green function $\hat{\underline{G}}(\mathbf{z})$ depending on the complex energy argument z as the resolvent of the Hamilton matrix $\hat{\underline{H}}$,

$$\hat{\underline{G}}(z)=\frac{\hat{\underline{1}}}{z\hat{\underline{1}}-\hat{\underline{H}}}\ , \tag{1}$$

the density of states in the mixed representation $n_{i\alpha}(\mathbf{K},E)$ is given by

$$n_{i\alpha}(\mathbf{K},E)=-\frac{1}{\pi}\mathrm{Im}\underline{G}_{i\alpha i\alpha}(\mathbf{K},E+i0)\ . \tag{2}$$

In our study we consider the projection on the first δ-

doping plane, labeled by $i=0$. Because of the periodicity perpendicular to the growth direction, all quantities of interest are diagonal in the wave vector $\mathbf{K}$. Within the mixed representation this property makes the system equivalent to a set of effective one-dimensional chains. Therefore, the $(\mathbf{K},i)$-resolved DOS displays square-root divergencies at the band edges typical for one-dimensional bands. This should be contrasted to the case of three-dimensional periodicity, where the introduction of the three-dimensional wave vector $\mathbf{k}$ reduces the problem of electronic structure calculations to that of a set of effective atomic clusters. To eliminate divergencies in the DOS a small imaginary part is added to the energy argument of the Green function.

In the case of bulk crystals the $(\mathbf{K},i)$-resolved DOS (often called projected bulk band structure) can be related to the bulk band structure. The $\mathbf{K}$ dependence is obtained by remapping the three-dimensional Brillouin zone (BZ) to a prismatic shape with the two-dimensional (2D) BZ as its basis and a z component varying from $-\pi/d$ to π/d, where d is the bulk interplane distance. The mixed representation is related to the Bloch basis formed with $\mathbf{k}$ vectors lying within this remapped 3D BZ by retaining the real-space description along the growth direction z instead of using the wave-vector component $\mathbf{k}_z$.

C. Koster-Slater approach to δ doping

We already stressed that the inclusion of a single monolayer impurity plane into a host material can be viewed as the limit of an ultrathin quantum well or the limit of infinitely large plane impurity clusters. Whereas the first approach is commonly used it is interesting to consider the latter equivalent point of view as well even if our calculation procedure does not follow this approach in detail.

First, we shortly repeat the case of a single deep impurity. Here, the main contributions to the impurity potential come from a small spatial region around the impurity atom. As a first approximation to the In impurity in GaAs we assume that only one on-site matrix element of the impurity potential $\underline{U}_{0s0s}$ is different from zero interpreted at the difference in atomic level position of the impurity and the host atom. Applying Green-function perturbation theory and employing the tetragonal symmetry at the defect site the projection of the Green function $\hat{\underline{G}}$ on the impurity site $I=0$ is given by

$$\underline{G}_{0s0s}(z)=\frac{\mathbb{1}}{\underline{G}^{(0)}_{0s0s}(z)^{-1}-\underline{U}_{0s0s}} , \tag{3}$$

where the subscript 0 denotes the Green function of the unperturbed lattice. Below the conduction-band edge $\underline{G}^{(0)}_{0s0s}$ is real and Eq. (3) simply states that the defect level is given by the intersection of $\underline{U}^{-1}_{0s0s}$ with the real part of the unperturbed Green function. It should be noted that the real part is connected with the spectral properties by a Hermitian transformation

$$\mathrm{Re}\underline{G}_{0s0s}(z)=\int_{-\infty}^{+\infty}\frac{n_{0s}(E)}{z-E}dE , \tag{4}$$

where $n_{0s}(E)$ is the local density of states projected on the s orbital on the impurity site. Therefore, defect levels reflect the density of states only indirectly. Generally, the real part of the matrix elements is negative below the conduction-band edge and starting from a certain negative value it reverses sign at some energy point in the band gap. Therefore, small enough impurity potentials do not lead to an impurity level inside the band gap in this approximation.

In the case of a δ-doping layer embedded in a host material the relevant impurity matrix elements are those in the mixed representation. Using the approximation made above only the matrix element of the impurity potential $\underline{U}_{0s0s}(\mathbf{K})$ is different from zero and in this special case it does not depend on $\mathbf{K}$. Due to the reduced symmetry, states with s and z orbital character mix and the analogous equations for the δ-doping case have matrix character. If we neglect this mixing near the $\bar{\Gamma}$ point we have

$$\underline{G}_{0s0s}(\mathbf{K},z)=\frac{\mathbb{1}}{\underline{G}^{(0)}_{0s0s}(\mathbf{K},z)^{-1}-\underline{U}_{0s0s}} , \tag{5}$$

$$\mathrm{Re}\underline{G}_{0s0s}(\mathbf{K},z)=\int_{-\infty}^{+\infty}\frac{n_{0s}(\mathbf{K},E)}{z-E}dE . \tag{6}$$

The level position now becomes $\mathbf{K}$ dependent, indicating the formation of impurity bands. In the case of a separated one-dimensional band the real part of $\underline{G}_{0s0s}(\mathbf{K},z)$ shows a square-root divergency at the band edge. Hence, impurity levels are formed for every value of the impurity potential. This statement is related to the fact that a square well contains at least one level. The situation is changed if the multiband character becomes important and different one-dimensional bands overlap.

In general, the single impurity detects global properties of the band structure of the host material whereas levels introduced by δ doping contain information about the surface band structure.

D. Evaluation of the Green function

In this section we describe the method used to calculate the Green-function matrix elements. It is based on the technique developed in Ref. 13 for the case of phonons in superlattices. More details on the application of Green functions to surfaces, interfaces, quantum wells, and superlattices may be found in Refs. 11 and 12. The formalism uses the diagonal form of all important quantities in the wave vector $\mathbf{K}$ that reduces the problem to that of an effective one-dimensional chain for every $\mathbf{K}$. The calculation proceeds in two steps. First, every such effective chain is divided into parts containing only one material. The host is characterized by two semi-infinite parts. Finite chains describing, e.g., the δ-doping layers or the GaAs well region are connected to these semi-infinite chains. The central quantities of our approach are Green-function matrix elements referring to the surface regions of these chains. They are calculated for the semi-infinite and every particular finite chain using a recurrence procedure. In the second step the individual chains are connected to one another until the required structure is obtained. To be explicit we describe the pro-

cedure for the case of GaAs with one δ-doping slab.

It is important to note that due to the restricted range of interaction between adjacent layers a so-called principal layer[11] can be defined. It is constructed by dividing the structure in small slabs of layers in such a way that every principal layer interacts only with its nearest neighbors. In the case of a tight-binding model with interactions up to second-nearest neighbors and the (100) growth direction the principal layer consists of the sequence anion-cation-layer, i.e., it contains two monolayers.

The recurrence procedure used to calculate the individual chains is closely related to that in Ref. 13. The analogy between the Green function for phonons [see Eq. (8) in Ref. 13 and for electrons Eq. (1)] makes a direct application of the technique described in Ref. 13 possible. In all formulas the terms $\underline{M}\omega^2$ have to be replaced by the energy argument $z\mathbf{1}$ and the force-constant matrix $\underline{F}$ by the corresponding matrix elements of the Hamiltonian. Note that, contrary to the Born model in Ref. 13, the tight-binding scheme used here considers interactions up to the second-nearest neighbors. Considering a chain of n principal layers, the projection of the Green function $\underline{\Gamma}_{(n)}$ to the surface subspace built up by a left (l) and a right (r) principal layer is a matrix of the range four times the number of orbitals per site, conveniently written as

$$\underline{\Gamma}_{(n)}=\begin{bmatrix}\underline{\Gamma}^{ll} & \underline{\Gamma}^{lr}\\ \underline{\Gamma}^{rl} & \Gamma^{rr}\end{bmatrix} . \tag{7}$$

We start with a chain of two principal layers and calculate the Green function $\underline{\Gamma}_{(2)}$ by direct application of Eq. (1). The surface projection of the Green function $\underline{\Gamma}_{(2n)}$ of a chain of doubled thickness can be calculated by Green-function perturbation theory closely following Eqs. (19)–(22) in Ref. 13. In this way finite chains are calculated. If the length of the finite chain is increased until no interaction between the surfaces exists it is taken as semi-infinite. The surface projection of the Green function $\underline{\Gamma}_{\infty}$ is diagonal,

$$\underline{\Gamma}_{(n)\infty}=\begin{bmatrix}\underline{\Gamma}^{ll}_{\infty} & \underline{0}\\ \underline{0} & \underline{\Gamma}^{rr}_{\infty}\end{bmatrix} . \tag{8}$$

In the second step a finite part is added to a semi-infinite chain. Explicitly we describe the connection of a δ-doping layer to the semi-infinite host chain. The surface Green-function matrix of the chain characterizing the δ-doping material of thickness n is denoted by $\underline{\Gamma}_{(n)\delta}$. Application of a Dyson equation yields for the matrix elements of the Green function projected on the top surface of the δ-doping slab $\underline{\Gamma}^{rr}_{(\infty+\delta)}$,

$$\underline{\Gamma}^{rr}_{(\infty+\delta)}=\underline{\Gamma}^{rr}_{\delta}+\underline{\Gamma}^{rl}_{\delta}\underline{V}^{(\delta,\infty)}\frac{\mathbb{1}}{(\underline{\Gamma}^{rr}_{\infty})^{-1}-\underline{V}^{(\infty,\delta)}\underline{\Gamma}^{ll}_{\infty}\underline{V}^{(\delta,\infty)}}\underline{V}^{(\infty,\delta)}\underline{\Gamma}^{lr}_{\infty} , \tag{9}$$

where $\underline{V}^{(\delta,\infty)}$ stands for the interaction matrix between the δ-doping layer and the semi-infinite chain. The last step adds the second semi-infinite chain of the host material. The projection of the Green function on the "right" surface of the δ-doping slab inside the host material $\underline{G}_{00}$ is given by

$$\underline{G}_{00}=\frac{\mathbb{1}}{(\underline{\Gamma}^{rr}_{(\delta+\infty)})^{-1}-\underline{V}^{(\delta,\infty)}\underline{\Gamma}^{ll}_{\infty}\underline{V}^{(\infty,\delta)}} . \tag{10}$$

In a similar way more complex arrangements may be constructed applying Eq. (9) repeatedly. Although looking at first complicated, the numerical afford is relatively small and can be handled on a personal computer easily.

III. RESULTS

A. δ doping of GaAs

This subsection is devoted to the discussion of the electronic structure of δ-doping layers embedded in pure GaAs. In Fig. 1 we show the $(\mathbf{K},i)$-resolved DOS projected on a Ga(001) layer in pure GaAs for energies near the conduction-band edge. The $\mathbf{K}$ vectors run along the two main symmetry lines $\bar{\Delta}$ and $\bar{\Sigma}$ in the 2D BZ. We display the projection on the s and z orbitals at the δ-doping layer. The one-dimensional character of bands with the singularities at the band edges is clearly visible. It should be noted that the point $\bar{\Gamma}$ represents essentially

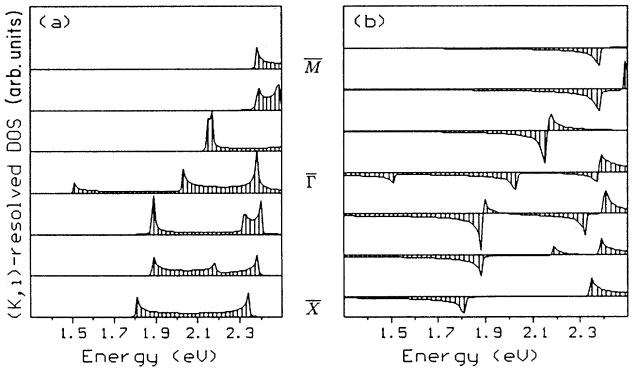

FIG. 1. $(\mathbf{K},i)$-resolved DOS at a Ga(001) layer in GaAs for $\mathbf{K}$ vectors along the $\bar{\Sigma}$ and $\bar{\Delta}$ line. Shown are the contributions of the $(s+z)$ orbitals (a). Real part of the Green-function matrix element $\underline{G}_{0s0s}$ for the same $\mathbf{K}$ vectors (b).

an integration of the bulk band structure along the Δ-(001) line. The band edge at point $\bar{X}$ is formed by states near L of the bulk band structure and the $\bar{M}$ point comprises the X ⟨100⟩ and ⟨010⟩ points. As expected, the conduction band starts with a well-separated band of (s) character centered near the $\bar{\Gamma}$ point. This band has low spectral weight due to the small effective mass except at the band edge. To get an insight into the development of defect states we show in Fig. 1(b) the real part of the Green-function matrix element $\underline{G}_{0s0s}(\mathbf{K},E)$ that determines, at least near $\bar{\Gamma}$, the defect level position for δ doping. Again, the functional form of the real part is related to that of a one-dimensional band with the typical square-root divergency at the edge. In Fig. 2 we show the ($\mathbf{K},i$)-resolved DOS projected on the In δ-doping layer embedded in pure GaAs. In addition to the s,z component the (x,y) contributions are displayed in Fig. 2(b). The formation of In-related defect levels below the band edges is well illustrated. As expected from the behavior of In impurities in bulk GaAs a comparison with Fig. 1(b) reveals that the defect potential is not very deep and the defect position is pinned by the singular form of the real part of the matrix element $\underline{G}_{0s0s}(\mathbf{K},E)$. Therefore, for $\mathbf{K}$ vectors near $\bar{\Gamma}$ the impurity level follows the dispersion of the GaAs bands. Figure 2(b) shows that In-related defect states have (s) character. Near the band edge no states of (x,y) symmetry are found. This is in correspondence with the observed polarization of the luminescence peaks.[4]

The one-dimensional character of the well-separated band forming the band edge of GaAs near $\bar{\Gamma}$ makes it possible to describe the system by a simple effective-mass model. This is the reason why the model of a square well used in simple interpretations of the experimental results works so well for this particular system.

The calculated dependence of the In-related defect state on the thickness of the In δ-doping slab at $\bar{\Gamma}$ is shown in Fig. 3. Noninteger coverages are modeled by an averaged concentration of impurity atoms. The parabolic dependence on the thickness for thin layers, found

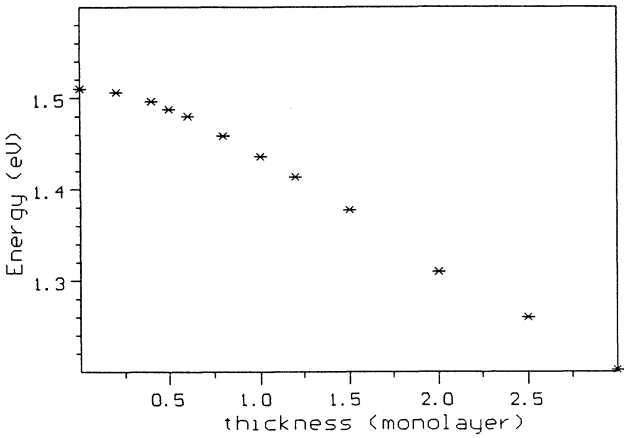

FIG. 3. Energy of the In-related defect level near the conduction-band edge at $\bar{\Gamma}$ dependent on the thickness of the δ-doping layer.

also experimentally,[14] is related to the inverse square-root behavior of the real part of the Green function near the band edge.

In the last part of this subsection we consider double δ doping by two monolayers of In separated by n layers of GaAs. The corresponding DOS at $\bar{\Gamma}$ projected on one In layer are shown in Fig. 4 for $n=1$, 2, 4, 8, 16, 32, and 64. Contrary to a single δ-doping layer, the defect positions contain information about the matrix elements $\underline{G}_{i\alpha j\alpha'}(\mathbf{K},z)$ of the Green function between different layers i and j. If both δ-doping layers are well separated, two degenerate levels are formed below the band edge. If the number of intermediate GaAs layers decreases, the hybridization between the wells splits the two levels into a bonding and an antibonding state. The splitting increases

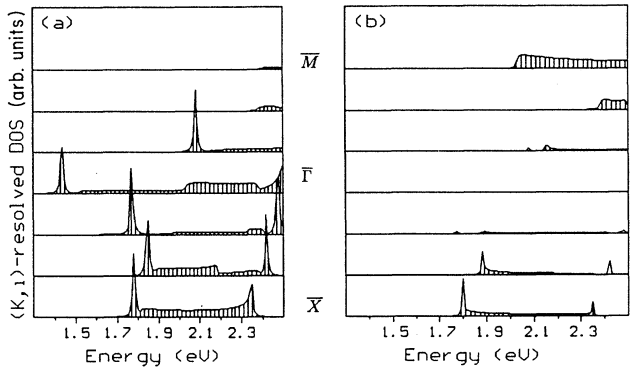

FIG. 2. ($\mathbf{K},i$)-resolved DOS at the In δ-doping plane embedded in GaAs for $\mathbf{K}$ vectors along the $\bar{\Sigma}$ and $\bar{\Delta}$ line. Shown are the contributions of (a) the ($s+z$), and (b) the ($x+y$) orbitals.

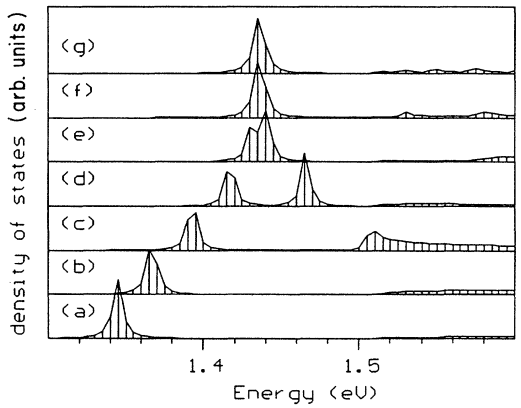

FIG. 4. Double δ doping of GaAs with In. Dependence of the ($\mathbf{K},i$)-resolved DOS on the number of GaAs layers n between the two δ monolayers. The number n is set to (a) 1, (b) 2, (c) 4, (d) 8, (e) 16, (f) 32, and (g) 64.

until the antibonding levels decay into the continuum of GaAs states and only a single level remains inside the band gap.

The calculated decrease of impurity levels with the thickness of the δ-doping slab and with decreasing distance between the two δ-doping layer in double δ doping cannot be directly related to energy differences of photoluminescence peaks. In this case, the electronic structure near the valence-band top has to be considered as well. Similarly, with increasing thickness of the δ-doping slab an increase of In-related defect states near the valence-band top is expected[10] making the redshift smaller than concluded from Figs. 3 and 4. In addition, the thickness dependence of exciton binding energies becomes important.[5,15] However, due to the only approximate description of the conduction bands within the tight-binding scheme the calculated energy differences are expected to be too large but show the correct qualitative trend. Here, recent pseudopotential calculations achieved a good fit to the experimental results.[7]

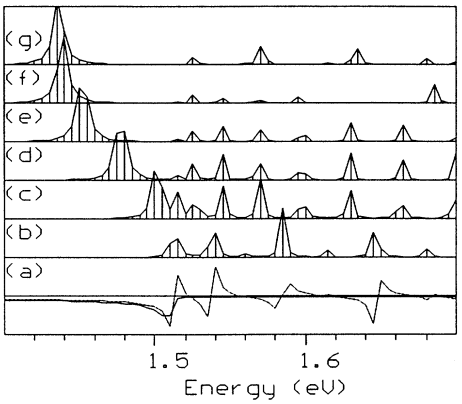

FIG. 5. Single δ doping of GaAs inside an AlAs/GaAs quantum well. Real part of the diagonal element of the Green function $\underline{G}_{0s0s}$ at $\bar{\Gamma}$ at a Ga layer in bulk GaAs (solid line) and at the Ga layer in the middle of an AlAs/GaAs (68 monolayer)/AlAs quantum well (dashed line) (a). $(\mathbf{K},i)$-resolved DOS at $\bar{\Gamma}$ projected on the $(s+z)$ orbitals of the Ga layer in the middle of a AlAs/GaAs (68 monolayer)/AlAs quantum well (b). $(\mathbf{K},i)$-resolved DOS at $\bar{\Gamma}$ projected on the $(s+z)$ orbitals of the In δ-doping layer embedded in the quantum well dependent on the distance i to the GaAs/AlAs interface for (c) $i=1$, (d) 2, (e) 4, (f) 8, and (g) 34 monolayers.

B. δ doping of AlAs/GaAs quantum wells

In this subsection we study δ doping of GaAs embedded in a single AlAs-GaAs-AlAs quantum well. The δ-doping In layer is now included in a nonperiodic system and, therefore, level positions will depend on the position of the δ-doping layer relative to the interfaces of the quantum well. We study the possibility to use the δ-doping layer as a local probe to the changed electronic structure of the GaAs inside the quantum well. The distance to the AlAs barrier gives another parameter to tune the energy of the photoluminescence peak.

Figures 5(b)–5(g) give a characteristic dependence of the DOS at $\bar{\Gamma}$ projected on the δ-doping layer in a AlAs/GaAs (68 monolayer)/AlAs quantum well in dependence on the position of the δ-doping layer relative to the interfaces. Figure 5(b) shows the DOS for the undoped quantum well. The formation of subbands below the AlAs conduction-band edge visible as (broadened) δ peaks in the $(\mathbf{K},i)$-resolved DOS is clearly seen. Below, in Fig. 5(a) the real part of the Green-function matrix element $\underline{G}_{0s0s}(\mathbf{K},z)$ is shown for a Ga layer placed inside pure GaAs (solid line) in comparison to that at the Ga layer in the middle of the quantum well (dashed line). For energies above the conduction-band edge of pure GaAs both are different but they nearly coincide below this energy. This illustrates that inside the quantum well the DOS is redistributed if compared to the bulk electronic structure but the balance of states determining the real part of the diagonal element of the Green function near the band edge remains nearly unchanged. Therefore, if the δ-doping layers are placed a sufficient distance from the interface to prevent interaction with AlAs states the position of the defect level is nearly the same as in pure GaAs and does not show any dependence on the subband structure. This is shown in Figs. 5(f) and 5(g).

In this case, if the δ-doping layer comes closer to the barrier an additional confinement increases the level positions. Figures 5(c)–5(f) show how the defect levels form below the first GaAs subband and collect for increasing distance from the barrier most of the spectral weight. The calculated dependence of the lowest peak on the distance is shown in Fig. 6 by crosses. The local character of the wave function related to the state confined inside the In δ-doping layer is reflected in the strong decay of

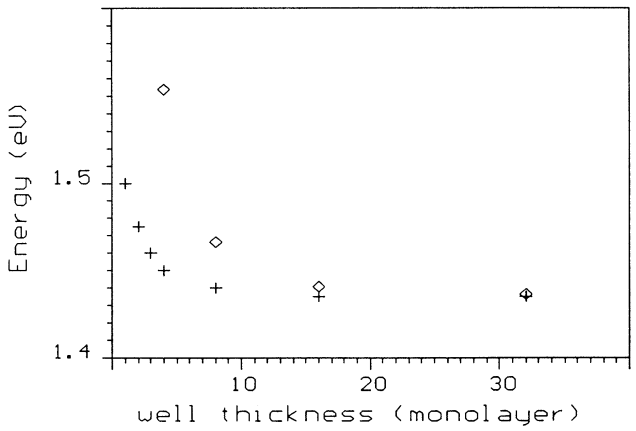

FIG. 6. Energy of the In-related defect level near the conduction-band edge at $\bar{\Gamma}$ for δ doping of the GaAs in the well region of a AlAs/GaAs quantum well dependent on the distance i to the interface. The crosses give results for a well thickness of 68 monolayer and the diamonds for a well thickness of $2i$.

the level position to the value found for δ doping in pure GaAs. This dependence on the distance is universal in the sense that it does not depend on the thickness of the well region for thicker quantum wells. On the other hand, it depends on the barrier potential and should be sensitive to the interface structure. It may be interesting to study this dependence in more detail.

If the quantum well is thin, the δ-doping layer interacts with both interfaces and the blueshift of the impurity level becomes larger. This is illustrated for δ-doping layers placed in the middle of a quantum well of thickness $2i$ where i is the distance to the interface. The resulting level positions are shown by diamonds. In pure AlAs the confinement becomes so strong that the In peak position, mostly determined by s-like states from the bulk Γ point, lies above the conduction-band edge formed by states related to the bulk X point. Hence, no photoluminescence signal will be found in In δ-doped AlAs.

IV. CONCLUSIONS

We studied the electronic structure at In δ-doping layers embedded in pure GaAs and inside the well region of a AlAs/GaAs single quantum well. The calculations are based on a tight-binding model combined with an effective scheme to obtain the density of states in the mixed representation.

We have shown that the well-separated, nearly parabolic and nondegenerate band forming the conduction-band edge of GaAs is related to a one-dimensional behavior of the $(\mathbf{K},i)$-resolved DOS near $\bar{\Gamma}$ with typical square-root divergencies of the real and imaginary part of diagonal matrix elements of the Green function. This quasi-one-dimensional behavior is responsible for the fact that an effective-mass description gives reasonable results even for ultrathin δ-doping layers. In contrast to the bulk case, where In does not induce a deep level in GaAs, the level positions are deeper in the δ-doping case due to the divergency of the real part of the Green function.

If the δ-doping layer is included in the GaAs well region of a AlAs/GaAs quantum well we found that the impurity level positions are not sensitive to the changed local electronic structure inside the GaAs well. Here, the additional confinement by the AlAs barriers induces an increase of levels related to δ doping if the δ-doping layer is placed near the interface. The actual level position depends on the distances to the interfaces and is expected to respond to the nature of the interface but not on details of the local electronic structure inside the well.

For a more detailed comparison with photoluminescence spectra the study has to be extended to the energy region near the valence-band top. This requires a more sophisticated description of the strain field and the inclusion of the spin-orbit interaction. Although this represents no serious problem the results will be sensitive to the actual models of the strain distribution, the band offsets, and impurity potentials that are connected with large uncertainties. A more quantitative analysis would, therefore, require more sophisticated calculation schemes.

[1]M. A. Tischler, N. G. Anderson, and S. M. Bedair, Appl. Phys. Lett. **49**, 1199 (1986).
[2]J. M. Gerhard and J. Y. Marzin, Appl. Phys. Lett. **53**, 568 (1988).
[3]K. Taira, H. Kawai, I. Hase, K. Kaneko, and N. Watanabe, Appl. Phys. Lett. **53**, 495 (1988); **55**, 1690 (1989).
[4]M. Sato and Y. Horikoshi, J. Appl. Phys. **66**, 851 (1989).
[5]O. Brandt, L. Tapfer, R. Cingolani, and K. Ploog, Phys. Rev. B **41**, 12 599 (1990).
[6]Q. Fu, D. Lee, A. V. Nurmikko, L. A. Kolodziejski, and R. L. Gunshor, Phys. Rev. B **39**, 3173 (1989).
[7]K. Shiraishi and E. Yamaguchi, Phys. Rev. B **42**, 3064 (1990).
[8]D. Hennig and S. Wilke, Proceedings of the Fifth International Conference on Superlattices and Microstructures, Berlin, 1990 [Superlatt. Microstruct. (to be published)].
[9]R. Strehlow, M. Hanke, and W. Kühn, Phys. Status Solidi **131**, 631 (1985).
[10]A. Taguchi and T. Ohno, Phys. Rev. B **39**, 7803 (1989).
[11]P. H. Lee and J. D. Joannopoulos, Phys. Rev. B **23**, 4988 (1981); **23**, 4997 (1981).
[12]F. García-Moliner and V. R. Velasco, Prog. Surf. Sci. **21**, 93 (1986).
[13]S. Wilke, J. Mašek, and B. Velický, Phys. Rev. B **41**, 3769 (1990).
[14]M. Sato and Y. Horikoshi, Appl. Phys. Lett. **55**, 1689 (1989).
[15]O. Brandt, R. Cingolani, L. Tapfer, G. Scamarcio, and K. Ploog, Proceedings of the Fifth International Conference on Superlattices and Microstructures (Ref. 8).